Journal of Pharmaceutical Analysis 14 (2024) 101036

Contents lists available at ScienceDirect

Journal of Pharmaceutical Analysis

journal homepage: www.elsevier.com/locate/jpa

Original article

Tetrandrine targeting SIRT5 exerts anti-melanoma properties via inducing ROS, ER stress, and blocked autophagy

Yacong Ji [a, b, 1], Chongyang Li [c, 1], Sicheng Wan [b, 1], Zhen Dong [b, 1], Chaolong Liu [b], Leiyang Guo [a], Shaomin Shi [a], Mingxin Ci [b], Minghao Xu [b], Qian Li [a], Huanrong Hu [a], Hongjuan Cui [b, d, e, **], Yaling Liu [a, *]

[a] Department of Dermatology, The Third Hospital of Hebei Medical University, Shijiazhuang, 050051, China
[b] State Key Laboratory of Resource Insects, Medical Research Institute, Southwest University, Chongqing, 400715, China
[c] Department of Medical Oncology, Shanghai Pulmonary Hospital, School of Medicine, Tongji University, Shanghai, 200433, China
[d] JinFeng Laboratory, Chongqing, 400715, China
[e] Engineering Research Center for Cancer Biomedical and Translational Medicine, Southwest University, Chongqing, 400715, China

ARTICLE INFO

Article history:
Received 13 January 2024
Received in revised form
10 June 2024
Accepted 1 July 2024
Available online 2 July 2024

Keywords:
Melanoma
Tetrandrine
Sirtuin 5 (SIRT5)
Mitophagy
Cytoskeletal protein depolymerization
Reactive oxygen species (ROS)

ABSTRACT

Tetrandrine (TET), a natural bisbenzyl isoquinoline alkaloid extracted from *Stephania tetrandra* S. Moore, has diverse pharmacological effects. However, its effects on melanoma remain unclear. Cellular proliferation assays, multi-omics analyses, and xenograft models were used to determine the effect of TET on melanoma. The direct target of TET was identified using biotin-TET pull-down liquid chromatography-mass spectrometry (LC-MS), cellular thermal shift assays, and isothermal titration calorimetry (ITC) analysis. Our findings revealed that TET treatment induced robust cellular autophagy depending on activating transcription factor 6 (ATF6)-mediated endoplasmic reticulum (ER) stress. Simultaneously, it hindered autophagic flux by inducing cytoskeletal protein depolymerization in melanoma cells. TET treatment resulted in excessive accumulation of reactive oxygen species (ROS) and simultaneously triggered mitophagy. Sirtuin 5 (SIRT5) was ultimately found to be a direct target of TET. Mechanistically, TET led to the degradation of SIRT5 via the ubiquitin (Ub)-26S proteasome system. SIRT5 knockdown induced ROS accumulation, whereas SIRT5 overexpression attenuated the TET-induced ROS accumulation and autophagy. Importantly, TET exhibited anti-cancer effects in xenograft models depending on SIRT5 expression. This study highlights the potential of TET as an antimelanoma agent that targets SIRT5. These findings provide a promising avenue for the use of TET in melanoma treatment and underscore its potential as a therapeutic candidate.

1. Introduction

Melanoma, known for its aggressive and metastatic potential, is one of the most lethal forms of skin cancer [1]. Early-stage melanoma traditionally requires surgical excision, whereas advanced-stage melanoma requires long-term therapeutic interventions, including chemotherapy, targeted therapy, and immunotherapy. Despite the initial success of dacarbazine was approved by the US Food and Drug Administration (FDA) in 1975 for the treatment of metastatic melanoma, its limitations, namely, resistance and modest efficacy, have posed significant hurdles [2]. With the development of personalized healthcare, targeted immunotherapies have attracted increasing attention. Targeted therapeutic drugs currently mainly include V-Raf murine sarcoma viral oncogene homolog B1 (BRAF) inhibitors (such as sorafenib and vemurafenib) [3], receptor tyrosine kinase (c-kit) inhibitors (including imatinib and nilotinib) [4,5], mitogen-activated extracellular signal-regulated kinase (MEK) inhibitors (such as trametinib and cobimetinib) [6,7], and vascular endothelial growth factor (VEGF) inhibitors (e.g., bevacizumab) [8]. Although targeted therapy exhibits high response rates and rapid effects, patients lacking these genetic mutations or amplifications still lack corresponding therapeutic drugs [9]. Furthermore, immune checkpoint inhibitors targeting programmed cell death receptor-1 (PD-1,

Peer review under responsibility of Xi'an Jiaotong University.
* Corresponding author.
** Corresponding author. State Key Laboratory of Resource Insects, Medical Research Institute, Southwest University, Chongqing, 400715, China.
E-mail addresses: hcui@swu.edu.cn (H. Cui), yzling_liu2023@hebmu.edu.cn (Y. Liu).
[1] These authors contributed equally to this work.

https://doi.org/10.1016/j.jpha.2024.101036

pembrolizumab), programmed cell death ligand-1 (PD-L1, nivolumab), and cytotoxic T lymphocyte-associated antigen-4 (CTLA-4, ipilimumab) [10] have demonstrated unprecedented durable response rates in cancer patients; however, the response rate is low (50%), and tumor reactions also require long time [11]. Therefore, the exploration of new therapeutic targets and development of corresponding therapeutic drugs for melanoma are urgently needed.

Tetrandrine (TET), a natural compound derived from traditional Chinese medicinal plants belonging to the family Menispermaceae, including *Stephania tetrandra* S. Moore and *Tinospora crispa* (L.) Hook. f. & Thomson and *Cyclea peltata* Diels, exhibits a diverse range of biomedical activities. Its notable effects encompass immunoregulation [12], inhibition of Ca^{2+} and Ca^{2+}-activated K^{+} channels [13], and antibacterial properties. Additionally, TET is promising for treating various diseases, including inflammatory conditions, cardiac and vascular ailments such as hypertension, and autoimmune disorders such as asthma, dysentery, hyperglycemia, tuberculosis, malaria, and fever.

Importantly, several studies have indicated that TET has an activity against multiple cancers, including oral, laryngeal, breast, liver, glioma, lung, leukemia, gastric, colorectal, pancreatic, prostate, endometrial, cervical, ovarian, and bladder cancers. The mechanisms underlying the anti-cancer effects of TET involve modulation of various genes and signaling pathways [14]. However, existing research tends to focus on broader signaling pathways without pinpointing specific molecular targets to fully elucidate the pharmacological mechanisms involved in the efficacy of TET in different human cancers.

In this study, we firstly investigated the anti-tumor potential of TET on melanoma. Our study used comprehensive *in vivo* and *in vitro* assays to assess the efficacy of TET against melanoma. Additionally, we sought to identify the precise target of TET within melanoma cells using biotin-TET pull-down coupled with liquid chromatograph-mass spectrometer (LC-MS) techniques, molecular dynamics simulation (MDS), and isothermal titration calorimetry (ITC) analysis. These methodologies aimed to shed light on the specific molecular mechanisms underlying the mode of action of TET in the context of melanoma, presenting a novel avenue for understanding and exploiting its therapeutic potential in this cancer type.

2. Materials and methods

2.1. Cell culture

The human melanoma cell lines A375 and SK-MEL-28, along with the human embryonic renal cell line HEK293T, were obtained from the American Type Culture Collection (ATCC; Rockville, MD, USA). MV3 cells were obtained from the University Hospital of Nijmegen [15]. A375, SK-MEL-28, and HEK293T cells were cultured in Dulbecco's modified Eagle's medium (DMEM; Biological Industries, Kibbutz Beit Haemek, Israel), and MV3 cells were cultured in Roswell Park Memorial Institute (RPMI) 1640 medium (Biological Industries). Both media were supplemented with 10% fetal bovine serum (FBS; Biological Industries) and 1% penicillin-streptomycin (New Cell & Molecular Biotech Co., Itd., Suzhou, China). Cells were cultured at 37 °C with 5% CO_2 in a humidified incubator (Sanyo, Osaka, Japan).

2.2. Drugs

TET, with a purity greater than 99%, was obtained from the MedChem Express (Cat. No.: HY-13764; Shanghai, China). AMG PERK 44, 4μ8C, melatonin (MT), chloroquine (CQ) and bafilomycin A1 (BafA1) were also obtained from the MedChem Express (Cat. Nos.: HY-12661A, HY-19707, HY-B0075, HY-17589A, and HY-100558). All drugs were dissolved in dimethyl sulfoxide (DMSO; Sigma-Aldrich®, Merck, St. Louis, MO, USA). 3-methyladenine (3-MA; Cat. No.: HY-19312), MG132 (Cat. No.:133407-82-6), cycloheximide (CHX; Cat. No.: 66-81-9) and N-acetylcysteine (NAC; Cat. No.: HY-B0215) were obtained from the MedChem Express. The two drugs were dissolved in deionized water. SF488 (Green)-conjugated phalloidin (Cat. No.: CA1640) was obtained from the Solarbio (Beijing, China). Tubulin-Tracker Red (Cat. No.: C1050) was purchased from the Beyotime (Shanghai, China).

2.3. 3-(4,5-dimethylthiazol-2-yl)-2,5-diphenyl tetrazolium bromide (MTT) assay

MTT (Sigma-Aldrich®, Merck) assay was performed to determine cell viability. A375 and MV3 cells were cultured in 96-well plates overnight. Approximately 1000 cells were seeded in 200 μL medium per well. After treatment with TET at the indicated concentrations, DMSO was used as the control. MTT (5 mg/mL, 20 μL per well) was added into the culture medium and then the plates were incubated at 37 °C for 4 h. Formazan was further dissolved with DMSO (200 μL). Finally, absorbance was measured using a spectrophotometer at a wavelength of 560 nm after shaking the well plates for 10 min.

2.4. 5-ethynyl-2'-deoxyuridine (EdU) staining

A375 and MV3 cells (about 2×10^4 cells per well) were cultured in 24-well plates overnight in a 37 °C incubator. They were then treated with TET alone or TET in combination with other drugs for another 48 h. DMSO was used as a control. EdU staining was performed by using the BeyoClick EdU Cell Proliferation Kit (Beyotime) according to the instructions provided by the manufacturer. The number of EdU-positive cells was observed and recorded using a fluorescence microscope (Olympus, Tokyo, Japan).

2.5. Trypan blue staining

A375 and MV3 cells were treated with DMSO or TET for 48 h. Following the corresponding experimental protocol, the trypan blue dye (Cat. No.: C0011; Beyotime) method was used to calculate the proportion of surviving cells.

2.6. Plate clone formation and soft agar assays

The cellular colony formation activity was determined using a plate clone formation assay. Melanoma cells were cultured in 6-well plates for 2 weeks. The medium was then removed and the cells were stained with 1% crystal violet solution (Cat. No.: C01221; Beyotime) for 5 min. Afterwards, the cells were washed gently with the phosphate buffered saline (PBS, Cat. No.: C0221A; Beyotime), and the plates were scanned using an Epson scanner (Nagano, Japan). Next, 1 mL of ethanol was added to each well of the plate and shaken for 5 min. Absorbance was measured using a Thermo Fisher microplate reader (Thermo Fisher Scientific, Waltham, MA, USA).

For the soft agar assay, melanoma cells were mixed with medium containing 0.6% agarose (Sigma-Aldrich®, Merk) and transferred into 12-well plates containing a solidified substrate (0.3% agarose in the medium). Colonies were imaged and counted after 2 weeks of growth.

2.7. Apoptosis assay and cell cycle assay

Apoptosis was detected by double staining with an Annexin V-FITC/PI Kit (abs50001; Absin, Shanghai, China) according to the manufacturer's instructions. The cell cycle was analyzed by staining with propidium iodide (BD, San Jose, CA, USA) and ribonuclease A (RNase A) (Sigma-Aldrich®, Merk), and the cells were harvested and fixed in 75% ethanol at 4 °C for 24 h. A Beckman CytoFLEX flow cytometer (Beckman Coulter, Indianapolis, IN, USA) was used to measure the signals, and FlowJo 7.6 software (FlowJo, Ashland, OR, USA) was used to analyze the proportion of cells in the cell cycle and apoptosis.

2.8. Western blot assay

Cells were collected using a cell scraper and lysed in radioimmunoprecipitation assay (RIPA) lysis buffer (Beyotime) for 20 min with 1 mM phenylmethanesulfonyl fluoride (PMSF; Beyotime). Then the samples were centrifuged at 14,000 r/min at 4 °C for 15 min, and the supernatant was collected, which was subsequently denatured by a metal-bather at 100 °C for 30 min. A standard curve was drawn using the bicinchoninic acid (BCA) method to determine protein concentration. Proteins were separated on 8%, 10%, or 12% sodium dodecyl sulfate-polyacrylamide gel electrophoresis (SDS-PAGE) gels respectively using a vertical electrophoretic apparatus (Bio-Rad, Hercules, CA, USA), and then transferred using semi-dry electrophoretic transfer (Bio-Rad) to a polyvinylidene difluoride (PVDF) membrane. The bovine serum albumin (BSA) was blocked at room temperature (RT) for 2 h. Then a primary antibody was incubated at 4 °C overnight. The anti-phosphorylation-AMP-activated protein kinase (anti-p-AMPK) (T172/T183) (Cat. No.: ab133448), p-mTOR(S2481) (Cat. No.: ab137133), p-mTOR(S2448) (Cat. No.: ab109268), cleaved poly (ADP-ribose) polymerase (c-PARP; Cat. No.: ab32064) and cleaved-caspase3 (c-caspase3; Cat. No.: ab2302) antibodies were purchased from the Abcam (Shanghai, China). Anti-*c*-caspase (Cat. No.: 9664) and β-actin (Cat. No.: 3700T) were purchased from the Cell Signaling Technology (Danvers, MA, USA). Anti-LC3B (Cat. No.: 314600-1-AP), UNC-52-like kinase 1 (ULK1; Cat. No.: 20986-1-AP), p62(18420-1-AP), Syntax 17 (Cat. No.: 17815-1-AP), glyceraldehyde-3-phosphate dehydrogenase (GAPDH; Cat. No.: 60004-1-Ig), Tubulin (Cat. No.: 66031-1-lg), activating transcription factor 6 (ATF6; Cat. No.: 24169-1-ap), inositol requiring enzyme 1 alpha (IRE1α; Cat. No.: 27528-1-AP), double-stranded RNA-dependent protein kinase-like ER kinase (PERK; Cat. No.: 24390-1-AP), CCAAT/enhancer-binding protein homologous protein (CHOP; Cat. No.: 15204-1-AP), phosphatase and tensin homolog (PTEN)-induced kinase 1 (PINK1; Cat. No.: 23274-1-AP), nuclear dot protein 52 kDa (NDP52; Cat. No.: 12229-1-AP), optineurin (OPTN; Cat. No.: 10837-1-AP), P53 up-regulated modulator of apoptosis (PUMA; Cat. No.: 55120-1-AP) and sirtuin 5 (SIRT5; Cat. No.: 15122-1-AP) were purchased from Proteintech (Wuhan, China). The PVDF membranes (Beyotime) were then washed three times with tris buffered saline with tween-20 buffer (TBST; Beyotime) and incubated with a secondary antibody, horseradish peroxidase (HRP)-labeled goat anti-mouse or rabbit IgG (Life Technologies, Carlsbad, CA, USA) at RT for 2 h. A Western blot imprinting instrument (Clinx Science, Shanghai, China) and enhanced chemiluminescence (ECL; Beyotime) were used to visualize the signals.

2.9. Immunofluorescence (IF) assay

An IF assay was performed to detect LC3B puncta and tubulin in A375 and MV3 cells. The cells were then incubated with LC3B (1:250; Cat. No.: 14600-1-AP; Proteintech) or Tubulin (1:50; Cat. No.: 10068-1-AP; Proteintech) at 4 °C overnight. The cells were then incubated with Alexa Fluor 488-conjugated goat anti-rabbit and 594-conjugated goat anti-mouse secondary antibodies (1:2000; Invitrogen, Carlsbad, CA, USA) at RT for 2 h. The 4',6-diamidino-2-phenylindole (DAPI; 1:500; Beyotime) was used to stain the nuclei.

2.10. Transmission electron microscopy (TEM)

Cells in 100 mm plates were treated with 10 μM TET or DMSO for 48 h and then the plates were washed three times with PBS and collected via trypsinization. The samples were washed three times with PBS and fixed with 2.5% glutaraldehyde (BL911A; Biosharp, Hefei, China) at 4 °C overnight. Then the samples were observed using a TEM by professionals in the Lilai Company (Chengdu, China).

2.11. Phalloidin staining of F-actin, Tubulin-Tracker Red staining of tubulin and MitoTracker Red staining of mitochondria

Cells were treated with TET alone or in combination with other drugs for the indicated time periods. The medium was then removed and the cells were washed three times with PBS. Afterwards, the cells were fixed with 4% paraformaldehyde (P-0099; Beyotime) in PBS for 30 min at 4 °C. The cells were then permeabilized with 0.2% Triton X-100 (ST1723; Beyotime) in PBS for 5 min and washed three times with PBS. Then cells were stained with SF488-conjugated phalloidin (1 μg/mL; Sigma-Aldrich®, Merk) or Tubulin-Tracker Red (C1050; Beyotime) for 20 min and fluorescent signals were visualized using confocal microscopy (FV1000; Olympus). The MitoTracker Red CMXRos (Cat. No.: C1035; Beyotime) was used to visualize mitochondria in live cells, according to the manufacturer's instructions.

2.12. Measurement of reactive oxygen species (ROS)

Adherent melanoma cells were treated with different drugs and then directly incubated with the 2',7'-dichlorodihydrofluorescein diacetate (DCFH-DA) probe (Cat. No.: S0033S; Beyotime), O13 Red probe (HR9097; BaiAoLaiBo, Beijing, China), dihydroethidium (DHE) probe (Cat. No.: S0063; Beyotime), MitoROS 580 probe (Cat. No.: 16052; AAT Bioquest, Xi'an, China), and MitoROS OH580 probe (Cat. No.: 16055; AAT Bioquest), according to the manufacturer's instructions. Next, the melanoma cells were washed with PBS. Subsequently, signals were captured under a fluorescence microscope. For detection using flow cytometry, the melanoma cells were resuspended and then the DCFH-DA probe was added with a final concentration of 10 μM. After separating and mixing, the cells and the probes were fully contacted. The cells were then washed and analyzed using the flow cytometry. Data were statistically analyzed and graphed using FlowJo 7.6 software.

2.13. Plasmid construction and transfection

For ATF6 and SIRT5 silencing, short hairpin RNA (shRNA) sequences were designed by using the siRNAext website (http://sirna.wi.mit.edu/), and then these designed silencing hairpin sequences were synthesized by BGI (Beijing, China) and cloned into a lentiviral pLKO.1 vector. For SIRT5 overexpression, the full-length coding sequence of SIRT5 was obtained from MV3 cells via polymerase chain reaction (PCR) by using the PrimeSTAR® Max DNA Polymerase (Takara Bio Inc., Beijing, China). The shRNA target sequences and primers used for PCR are listed in Table S1. This was then ligated into the pCDH-CMV-MCS-EF1-puro vector. Afterwards, pCDH-CMV-MCS-EF1-puro-SIRT5 and packaging plasmids (pLP1, pLP2, and PLP/

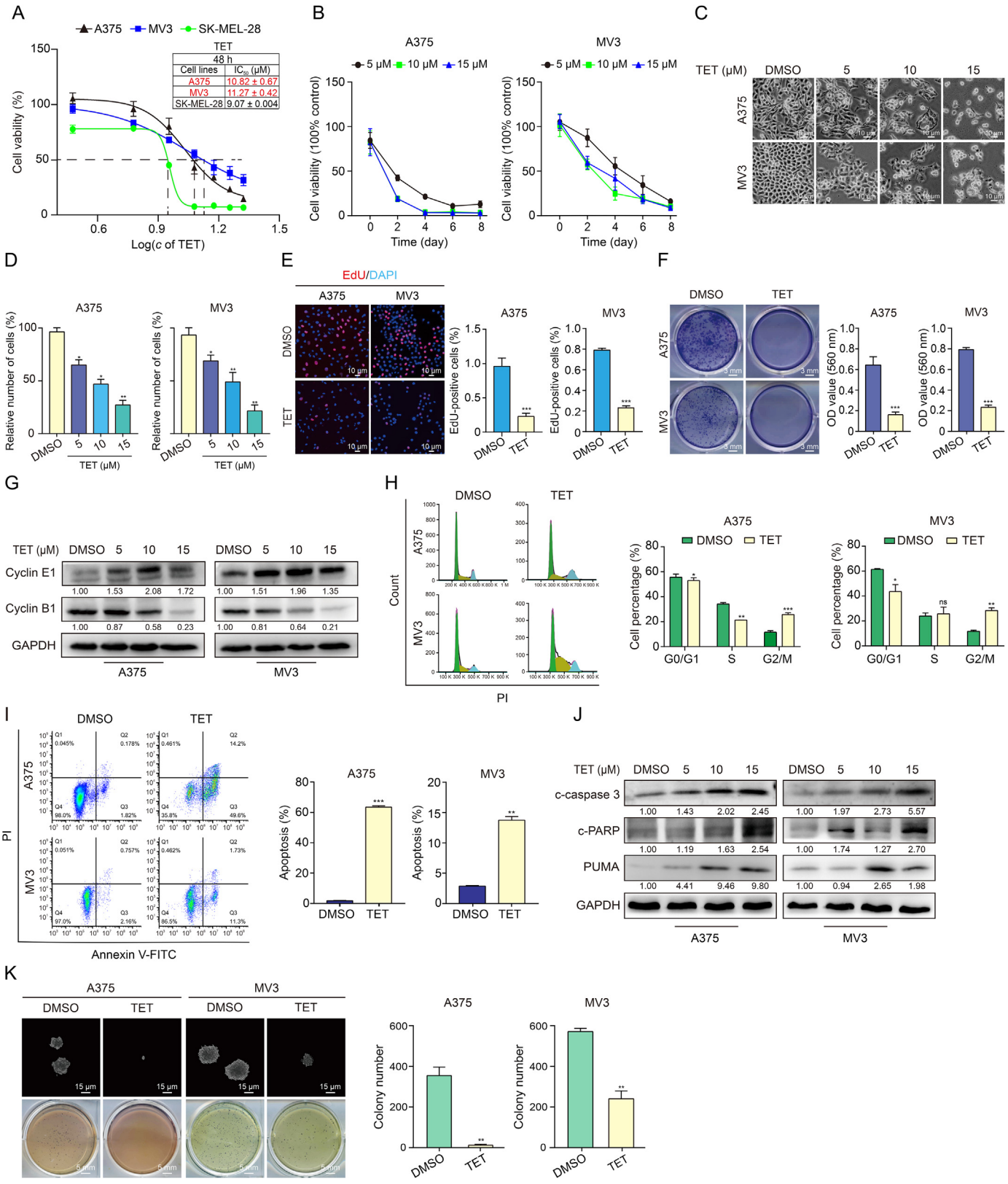

Fig. 1. Tetrandrine (TET) inhibited cell proliferation and viability in melanoma cells. (A) Melanoma cells (A375 and MV3) were incubated with a series of different TET concentrations for 48 h. Cell viability was measured by the 3-(4,5-dimethylthiazol-2-yl)-2,5-diphenyl tetrazolium bromide (MTT) assay. The half-inhibitory concentrations (IC_{50}) values of TET for 48 h in the both cell lines were marked in the upper right corner. (B) Viability of A375 and MV3 cells was tested after treated with TET. (C, D) Morphology of A375 and MV3 cells under different TET concentrations of treatment (5, 10 and 15 μM) for 48 h (C), and Histograms show the effect of TET on the viability of the cells (D). (E) 5-ethynyl-2'-deoxyuridine (EdU) assay evaluated the proliferation capacity of cells treated with dimethyl sulfoxide (DMSO) or TET (10 μM) for 48 h. Quantity of EdU-positive A375 and MV3 cells were calculated. (F) Clonogenicity of A375 and MV3 cells was assessed after treated with DMSO or TET (10 μM). The colonies were cultured for 7 days. Crystal violet was solved by 75% ethyl alcohol and the absorbance of each well was assessed by microplate reader (560 OD). (G) Western blot assay detected the expression of cell cycle-related proteins after

VSVG) were transfected into 293FT cells to construct lentiviruses using the Lipofectamine Lipo2000 transfection reagent (Life Technologies). The viral supernatant was collected and used to infect A375 and MV3 cells using 5 μg/mL polybrene. After infection, the cells were treated with 2 μg/mL puromycin (A1113803; Life Technologies) twice to select the alive cells.

2.14. Green fluorescent protein (GFP)-Red fluorescent protein (RFP)-LC3 plasmid transient transfection

The GFP-RFP-LC3 plasmid was transfected into A375 and MV3 cells using the ViaFect transfection reagent (Promega, Madison, WI, USA). The transfected cells were grown on coverslips in 24-well plates and treated with TET alone or in combination with other drugs for 48 h. The cells were then washed with PBS and fixed with 4% paraformaldehyde for 15 min. The cells were then permeabilized with 0.1% Triton X-100 for 5 min. DAPI (1:500; Beyotime) was used for nuclear staining. The cells were observed under a confocal laser scanning microscope (Olympus). The detailed protocol has been described previously [16].

2.15. Reverse transcription-quantitative PCR (RT-qPCR)

The RT-qPCR was performed as previously described [17]. The primers used are listed in Table S2.

2.16. Cellular thermal shift assay

The thermal shift assays were used to study the thermal stabilization of the proteins upon ligand binding. A375 and MV3 cells were collected, washed with PBS, re-suspended in pre-cooled PBS, supplemented with protease inhibitors, treated with liquid nitrogen for 3 min, incubated at RT for 3 min, and circulated three times. The samples were centrifuged at 4 °C, 13,000 rpm for 15 min, and supernatants were divided equally into two eppendorf tubes and added to TET or DMSO, respectively. Samples were incubated for 30 min and transferred to PCR tubes. The tubes were heated in a PCR instrument at the indicated temperatures for 3 min. The supernatant was then centrifuged again. Proteins were detected and quantified by using the Western blot analysis.

2.17. RNA sequencing (RNA-seq) and analysis

MV3 and A375 cell lines were cultured in 100 mm dishes and treated with 10 μM TET. After 48 h, the cells were collected and stored in the TRIzol reagent (Invitrogen). RNA integrity tests, library construction, next-generation sequencing (NGS), mapping, and gene expression qualification were performed by the Biomarker Company (Beijing, China). All analysis and visualizations were performed using the R software (version 3.6.3; Bell Laboratories, New Providence, NJ, USA). The Rpackage "Limma" was conducted to screen the differential expression genes (DEGs) between the two groups (DMSO vs. TET) among the two cell lines, according to the following criteria: false-discovery rate (FDR; Benjamini Hochberg method) $\leq$0.001 and Log2 (fold change) $\geq$1. Gene set enrichment analysis (GSEA) was performed by R-package "ClusterProfiler" (Geneset database: MSigDB Collection (https://www.gsea-msigdb.org/gsea/msigdb/index.jsp)) and visualized in mountain plot. As for gene ontology (GO) enrichment, we screened the co-upregulated genes in both cells using the R-package "VennDiagram" and identified 257 such genes. GO enrichment analysis was performed by R-package "ClusterProfiler" based on these co-upregulated genes. The expression of SIRT5 between normal and melanoma patient tissues from Genotype-Tissue Expression (GTEx) and The Cancer Genome Atlas (TCGA) databases, along with the patients' prognosis with different SIRT5 expression (low vs. high) were evaluated using the online database Gene Expression Profiling Interactive Analysis (GEPIA2; http://gepia2.cancer-pku.cn/#index).

2.18. ITC analysis

The binding affinities and thermodynamics of SIRT5 protein to TET were determined using the MicroCal PEAQ-ITC (Malvern Panalytical, Worcestershire, UK). Before each measurement, all the solutions were degassed to avoid air bubbles. Then SIRT5 (50 μg, 300 μL) in sodium phosphate buffer (300 mM NaCl and 20 mM Na2HPO4, pH 7.4) was loaded in the ITC cell at 25 °C. TET (100 μM, 200 μL) in the same buffer at 25 °C was titrated (10 μL each time) into the cell through a syringe, except for the first injection (2 μL). Data were analyzed by MicroCal PEAQ-ITC Analysis Software to determine binding parameters, including the association constant (K_D), enthalpy value (ΔH), and entropy value (ΔS).

2.19. Biotin-TET pull down/LC-MS

The biotin-TET-labeled probe, synthesized by Shanghai Targets Company (Shanghai, China), was directly incubated with the A375 cell lysate, and a pull-down assay was performed. The pull-down product was subjected to the Western blot validation and separated by SDS-PAGE. Coomassie brilliant blue (CBB) staining was performed, and the indicated gel strips were cut for LC-MS detection (Bioprofile, Shanghai, China).

2.20. MDS

The protein sequence and structure of SIRT5 were queried using the UniProt website (https://www.uniprot.org/uniprotkb/P00533/entry). The structure of TET was downloaded from the PubChem database. The docking software, Smina, was used. The conformations obtained after docking were used as the initial conformations for the kinetic simulations. Gromacs 2019.6 software was used for the kinetic simulation. Aber14sb was chosen as the protein force field, and the Gaff 2 force field was chosen for the small molecules. The TIP3P water model was added to the complex system, a water box was established, and sodium ions were added to equilibrate the system. Under elastic modelling by the Verlet and cg algorithms, the pectin methylesterase (PME) deals with electrostatic interactions using the steepest descent method for energy minimization at the maximum number of steps (50,000). The cutoff distances of the Coulomb force and van der Waals radius are both 1.4 nm. Finally, the system was equilibrated using a normal-variable system.

treated with different concentrations of TET. (H) The cell cycle of A375 and MV3 cells after treated with TET (10 μM) were detected by flow cytometry. Relative proportions of cells in different phases were presented in bar charts. (I) Apoptosis of A375 and MV3 cells after treated with TET (10 μM) for 48 h. Apoptosis rate was presented in bar charts. (J) Western blot assay detected the expressions of apoptosis-associated proteins in melanoma cells after treating with DMSO and TET (5, 10, and 15 μM). (K) The self-renewal capability of melanoma cells was investigated by soft agar assay after incubating with DMSO or TET (10 μM) for 14 days. All data were analyzed by unpaired Student's *t*-tests and shown as the means ± standard deviation (SD). $^{*}P < 0.05$, $^{**}P < 0.01$, $^{***}P < 0.001$, ns: not statistically significant. DAPI: 4',6-diamidino-2-phenylindole; FITC: fluorescein isothiocyanate; PI: propidium iodide; c-PARP: cleaved poly (ADP-ribose) polymerase; PUMA: P53 up-regulated modulator of apoptosis; DAPDH: glyceraldehyde-3-phosphate dehydrogenase; OD: optical density.

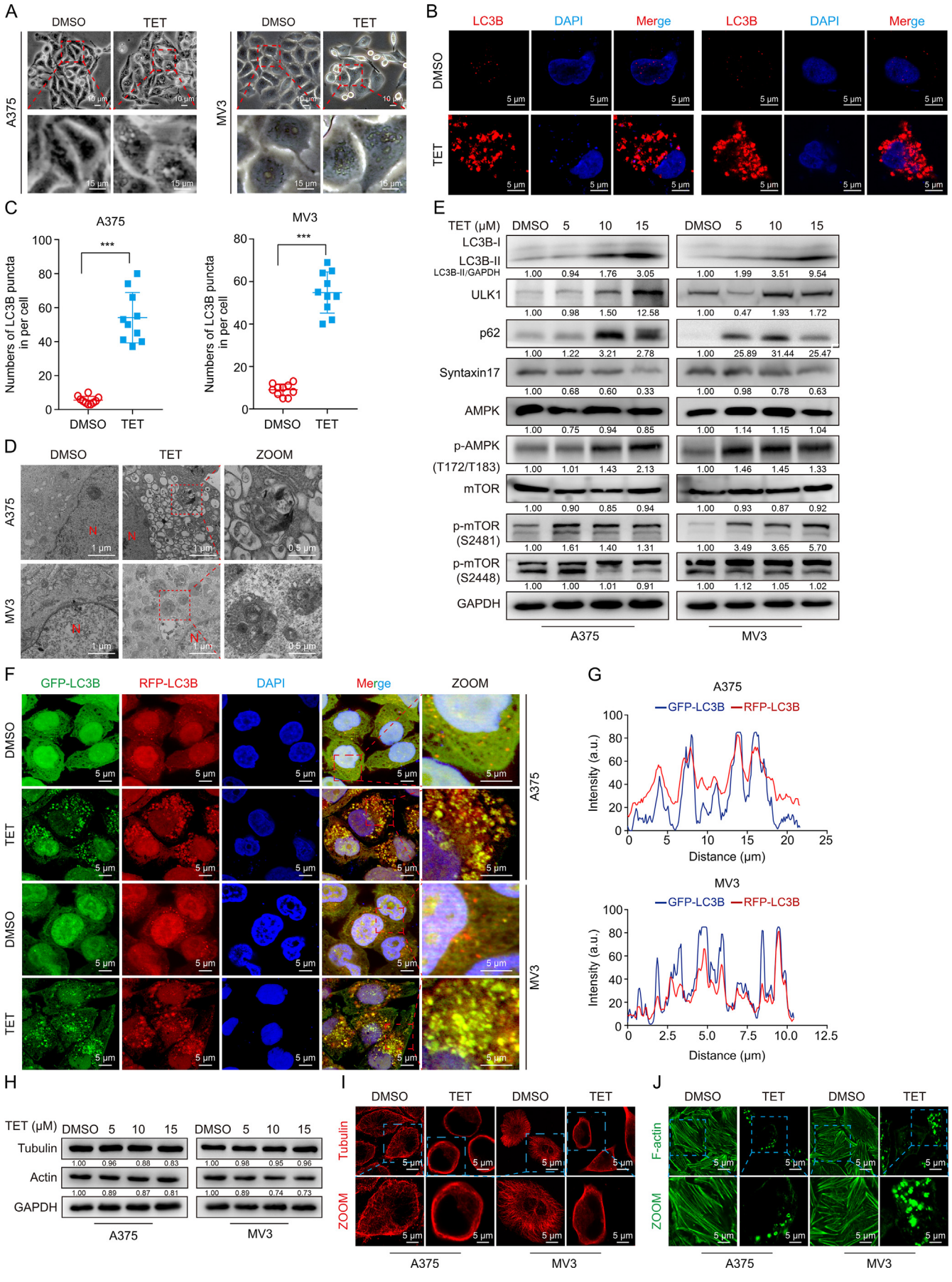
A
DMSO
TET
A375
MV3
10 μm
15 μm
B
LC3B
DAPI
Merge
5 μm
C
A375
MV3
Numbers of LC3B puncta in per cell
***
D
ZOOM
N
1 μm
0.5 μm
E
TET (μM)
LC3B-I
LC3B-II
LC3B-II/GAPDH
ULK1
p62
Syntaxin17
AMPK
p-AMPK (T172/T183)
mTOR
p-mTOR (S2481)
p-mTOR (S2448)
GAPDH
F
GFP-LC3B
RFP-LC3B
G
Intensity (a.u.)
Distance (μm)
H
Tubulin
Actin
I
J
F-actin

2.21. In vivo tumor xenograft assay

Animal experiments in this study were pre-approved and supervised by the Institutional Animal Care and Use Committee of Southwest University and the Experimental Animal Care and Use Committee of the Institute of Sericulture and Systems Biology (Approval No.: LAC2022-1-0018). A total of twenty-four female BALB/c-nu mice (4-week-old) were purchased from Hunan SJA Laboratory Animal Co., Ltd. (Changsha, China) and housed in a specific pathogen free (SPF) room for one week. Twelve mice were used to study the effect of MT on A375 melanoma xenograft cells. A375 cells (1×10^6) in 100 μL PBS were subcutaneously injected into the flanks of mice. They were then divided into four groups (a. DMSO; b. TET: 120 mg/kg/day; c. MT: 60 mg/kg/day; d. TET + MT: 120 mg/kg/day+60 mg/kg/day), and every group contained three mice. Twelve mice were used to the study of SIRT5 effect on A375 melanoma xenograft cells. A375 cells (1×10^6) with or without SIRT5 overexpression in 100 μL PBS were subcutaneously injected into the flanks of mice, which were then divided into four groups (a. vector (V) + DMSO; b. V + TET: 120 mg/kg/day; c. SIRT5+DMSO; d. SIRT5+TET: 120 mg/kg/day), and every group contained three mice. Each group was dealt with different treatment via intraperitoneal injection every 2 days for 30 days. Tumor volumes were measured using calipers every 5 days for 25 days. The tumor volume was calculated by the formula: Volume = tumor length × width^2 × π/6. At the end of the experiment, all animals were euthanized using CO_2. Subcutaneous tumors were removed and weighed.

2.22. Immunocytochemistry (IHC) assay

IHC assay was performed as described previously. Anti-SIRT5 Rabbit monoclonal antibody (Cat. No.: 15122-1-AP; Proteintech), Ki67 (Cat. No.: 550609; BD Biosciences) antibody, and Histostain™-SP Kits (Cat. No.: SPN-9002; ZSGB-BIO, Beijing, China) were used in this experiment [18].

2.23. Statistical analysis

All experiments were repeated at least three times. Data were analyzed and graphs were drawn using the GraphPad Prism 6. Data were presented as the mean ± standard deviation (SD). An unpaired two-tailed Student's *t*-test was used to analyze significant differences between the two groups. One-way analysis of variance (ANOVA) followed by Dunnett's test or Tukey's test was performed to compare the mean of each experimental group with that of the control group or to compare each group with the mean of every other group when performing multiple comparisons, respectively. $P < 0.05$ was considered statistically significant difference.

3. Results

3.1. TET inhibited cell proliferation and viability in melanoma cells

To evaluate the anti-melanoma effects of TET, we performed a series of assays using multiple melanoma cell lines. Initial determination of half-inhibitory concentrations (IC_{50}) of TET in A375, MV3, SK-MEL-28, p53-induced gene 1 (PIG1) and Hacat cell lines revealed IC_{50} values of 10.82±0.67 μM, 11.27±0.42 μM, 9.07±0.004 μM, 26.41±2.12 μM, and 23.32±3.08 μM, respectively (Figs. 1A and S1A). Subsequently, the A375 and MV3 cell lines displaying relatively minor differences in IC_{50} values were selected for further investigation. *In vitro* growth curve assays at different TET concentrations (5, 10, 15 μM) demonstrated a marked anti-proliferative effect on melanoma cells (Fig. 1B), accompanied by observable morphological changes (Figs. 1C and D). Further investigations using the EdU assay, colony formation assay, and cell cycle analysis revealed significant suppression of proliferation and G2/M phase cycle arrest upon TET treatment (Figs. 1E–H). Trypan blue staining and apoptosis-based flow cytometry confirmed TET-induced dose-dependent cell death (Fig. S1B). The Western blot analysis corroborated these findings, showing increased levels of apoptotic proteins including c-caspase3, c-PARP, and PUMA (Figs. 1I and J). Additionally, the soft agar assay underscored the reduced clone formation ability of melanoma cells after TET exposure (Fig. 1K). Collectively, these results comprehensively demonstrated the potent anti-melanoma efficacy of TET, which was attributed to its ability to suppress proliferation and induce apoptosis in melanoma cells (Figs. S1C–E).

3.2. TET induced a blocked autophagic flux via inducing cytoskeleton depolymerization

Upon TET treatment, discernible irregular vacuoles were observed within the cells, closely resembling autophagic vacuoles, suggesting the potential for the induction of cellular autophagy (Fig. 2A). To test this hypothesis, IF and TEM were performed. Compared with the control group, pronounced LC3B signals (highlighted in red) and vesicular structures akin to autophagosomes were notably prevalent (Figs. 2B–D). Cells expressing GFP-LC3B consistently exhibited similar patterns (Fig. S2A). Moreover, Western blotting was used to gauge the expression levels of autophagy-associated molecular markers under various concentrations of TET. As anticipated, there was a conspicuous upregulation in the expression of autophagic markers including LC3B, ULK1, and p-AMPK (T172/T183), confirming that TET induced autophagy in melanoma cells (Fig. 2E). However, the upregulation of p62, a recognized autophagic receptor, indicated the potential blockade of TET-induced autophagic flux (Fig. 2E). This was further supported by the downregulation of syntaxin 17, a protein pivotal in facilitating the fusion of autophagosomes with lysosomes, aligned with the increased expression of p62 (Fig. 2E). Moreover, upon TET treatment, a substantial number of co-localization signals were evident in cells expressing GFP-RFP-LC3B (a dual-labeled autophagic vector system), reinforcing the evidence of impaired autophagic flux (Figs. 2F, 2G and S2B).

Previous studies have established that concurrent initiation and blockage of autophagy can lead to cell death. Consequently, we aimed to elucidate whether this phenomenon contributes to TET-induced melanoma cell death. After combined treatment with TET and the autophagy inhibitors 3-MA, BafA1, or CQ individually, it was

Fig. 2. Tetrandrine (TET) induced autophagic flux blockage by destroying cellular cytoskeletal structure. (A) Cell morphology of A375 and MV3 cells was observed after treated with dimethyl sulfoxide (DMSO) or TET (10 μM) for 48 h. (B, C) Immunofluorescence (IF) assay tested the expression of LC3B in A375 and MV3 cells after treated with DMSO or TET (10 μM) for 48 h (B), and the nuclei were counterstained with 4',6-diamidino-2-phenylindole (DAPI) (blue), and the histogram showed the quantity of LC3B puncta in per cell (C). 10 cells were counted in each group. (D) The transmission electron microscopy (TEM) images of autophagosomes in A375 and MV3 cells after treated with DMSO or TET (10 μM) for 48 h. (E) Western blot assay detected the expressions of autophagy-associated proteins after treated with DMSO or TET (5, 10, and 15 μM) for 48 h in A375 and MV3 cells. (F, G) IF assay detected the level of autophagy after treated with TET (10 μM) for 48 h was tested in A375 and MV3 cells with stable-transfected green fluorescent protein (GFP)-red fluorescent protein (RFP)-LC3 (F), and the intensity of green and red signals in cells per slide were calculated by ImageJ software (G). (H) Western blot assay detected the expressions of tubulin and actin after treated with DMSO or TET (5, 10, and 15 μM) for 48 h in A375 and MV3 cells. (I, J) Microtubules (tubulin) and microfilament (F-actin) morphology were observed in A375 and MV3 cells after treated with TET (10 μM) for 48 h. All data were analyzed by unpaired Student's *t*-tests and shown as the means ± standard deviation (SD). $^{***}P < 0.001$. ULK1: UNC-52-like kinase 1; AMPK: AMP-activated protein kinase; p-AMPK: phosphorylation-AMPK; GAPDH: glyceraldehyde-3-phosphate dehydrogenase.

observed that while 3-MA effectively inhibited autophagic initiation, it failed to rescue TET-induced cell death (Figs. S2C and D). Similarly, BafA1 and CQ, which are inhibitors of late-stage autophagic processes, were unable to further augment TET-induced autophagic flux, substantiating the contention that TET triggers blocked autophagy (Figs. S2C, E, and F). Recognizing the critical role of the microtubule and microfilament systems in orchestrating the formation, transport, and fusion of autophagosomes with lysosomes [19–21], we investigated whether TET perturbed their normal structure. The results demonstrated that while TET marginally decreased the expression of tubulin and actin, it severely disrupted their structural integrity within melanoma cells (Figs. 2H–J). These findings suggested that TET-induced cytoskeletal depolymerization contributed to the blockade of autophagic flux.

3.3. TET induced autophagy via triggering endoplasmic reticulum (ER) stress

Based on the RNA-seq signaling pathway enrichment analysis, TET promoted the unfolded protein response (UPR) (Figs. 3A and B). Given the established association between autophagy and ER stress in extensive literature, we conducted TEM experiments, which revealed noticeable ER swelling (Fig. 3C). Simultaneously, the expression of pertinent ER stress markers, ATF6, IRE1α, PERK, and CHOP, showed significant upregulation (Fig. 3D). To explore the intricate relationship between autophagy and ER stress in melanoma cells, we combined TET with three distinct inhibitors, MT, 4μ8C, and AMG PERK 44, in the ER stress pathway. Interestingly, among these groups, only TET combined with MT, an ATF6 inhibitor, notably accelerated cell death and substantially suppressed cell proliferation (Figs. 3E and F). These results were consistently validated by various assays, including MTT, EdU, colony formation, and apoptosis-based flow cytometry (Figs. S3). Moreover, in a subcutaneous transplantation mouse model of melanoma cells, the combination of TET and MT significantly impaired tumor growth (Figs. 3G–J). Subsequently, we investigated whether TET-induced autophagy stems from ATF6-mediated ER stress using Western blotting. Notably, compared to TET treatment alone, the combination of TET and MT resulted in a marked decrease in autophagy in A375 cells (MV3 cells exhibited an inconclusive response). ATF6 knockdown inhibited TET-induced autophagy, further substantiating the findings above (Fig. 3K). In summary, these results strongly suggested that ATF6-mediated ER stress activates autophagy in TET-treated melanoma cells.

3.4. TET brought about massive ROS accumulation

To unravel the mechanisms underlying TET-induced ER stress and the consequent blockade of autophagy, we investigated its impact on ROS, a primary phenotype identified via RNA-seq analysis (Figs. 3A and B). Following TET exposure, alterations in mitochondrial morphology were evident, as marked by notable swelling and vacuolization (Fig. 4A). Intriguingly, substantial co-localization signals between LC3B and mitochondria were observed in the TET treatment groups, surpassing those in the control group (Fig. 4B). This phenomenon was corroborated by an increase in the expression of mitophagy-associated markers (PINK1, NDP52, and OPTN) (Fig. 4C). Collectively, these findings strongly indicate the activation of mitophagy following TET treatment. After TET treatment, a surge in ROS signals (detected using DCFH-DA; represented in green) was observed (Fig. 4D). We conducted an in-depth assessment of various ROS types, including total cellular ROS, O_2^-, MitoROS (O_2^-), and MitoROS (OH^-) (Figs. 4E–H). Surprisingly, concomitant with the surge in ROS levels, we observed TET-induced cell death, suppression of cell proliferation, cytoskeletal depolymerization, and blocked autophagic flux, all of which were effectively rescued by treatment with the ROS scavenger NAC (Figs. 4I–M). To further substantiate these findings, Western blot assay unveiled that the expression levels of key proteins associated with ER stress (ATF6, IRE1a, and PERK), apoptosis (c-PARP), mitophagy (PINK1 and NDP52), and autophagy (LC3B and p62) were reversed upon NAC treatment (Fig. 4N). Given that ROS is primarily generated within mitochondria, we hypothesized that TET-induced melanoma cell death results from mitochondrial dysfunction and subsequent ROS release, precipitating a cascade of cellular stress responses.

3.5. SIRT5 was identified as a direct target of TET

To elucidate the specific mechanism underlying TET-induced melanoma cell death, we identified the molecular targets of TET in cells. For the synthesis of biotin-labeled TET (Figs. 5A, S4, and S5), we confirmed that biotin-TET mirrored the properties of TET, displaying anti-melanoma proliferation and activation of autophagic flux, as corroborated by both MTT and IF experiments (Figs. 5B and C).

Subsequently, we employed the biotin-TET pulldown LC-MS to screen for potential TET targets (Figs. 5D and E, and Table S3). By integrating protein subcellular localization (mitochondria) and GO enrichment analysis of the pulldown proteins, SIRT5 emerged as a promising target (Fig. 5F). Competitive binding experiments validated the interaction between TET and SIRT5, demonstrating the dose-dependent competitive binding of TET with the initially interacting recombinant SIRT5 protein tagged with biotin-TET (Fig. 5G).

Augmenting our findings, bulk gene expression profiling in patients with melanoma substantiated that SIRT5 exhibits increased expression in melanoma tissues, correlating with poor patient prognosis (Fig. 5H). Notably, TET effectively downregulated SIRT5 expression in melanoma cells through Ub-26S proteasome system (UPS) mediation, although the change in messenger RNA (mRNA) levels was not significant (Figs. 5I–K, S6, and S7A).

Further verification via a cellular thermal shift assay and ITC experiments confirmed that SIRT5 was a direct molecular target of TET (Figs. 5L and M). MDS revealed the binding pattern between SIRT5 and TET, locating TET within the middle cavity (2 α-helixes and 2 β-sheets) of SIRT5 (forming hydrogen bond connections: Ser-178; Hydrophobic forces: Tyr176, Lys148, Gln144, Gly110, Phe162, and Lys 177) (Figs. 5N and O). These findings collectively indicate that SIRT5 is the primary driver of ROS accumulation in melanoma cells treated with TET.

3.6. TET impeded melanoma growth in vivo in a SIRT5-dependent manner

To validate the role of SIRT5 in TET-induced melanoma cell death, we generated SIRT5 knockdown cells (Fig. 6A). Significantly, ROS accumulation was evident in SIRT5 knockdown cells after TET treatment (Figs. 6B–F). Results of the Western blotting analysis showed that TET treatment of SIRT5-depleted cells markedly expanded TET-induced cellular stress cascades. Conversely, this stress response was notably alleviated in cells overexpressing SIRT5 (Figs. 6G and H). We conducted the ROS accumulation in shSIRT5 and overexpressing SIRT5 melanoma cells after treated with TET (10 μM). These results indicated that SIRT5 overexpression reversed TET-induced mitochondrial damage in melanoma cells (Figs. S7B–E). The TEM images of the mitochondria were also consistent (Fig. S7F).

Because TET showed a potent anti-tumor effect in melanoma cells *in vitro*, we attempted to confirm its efficacy in animal models. In a subcutaneous transplantation mouse xenograft model, TET treatment profoundly suppressed tumorigenicity, as evidenced by a

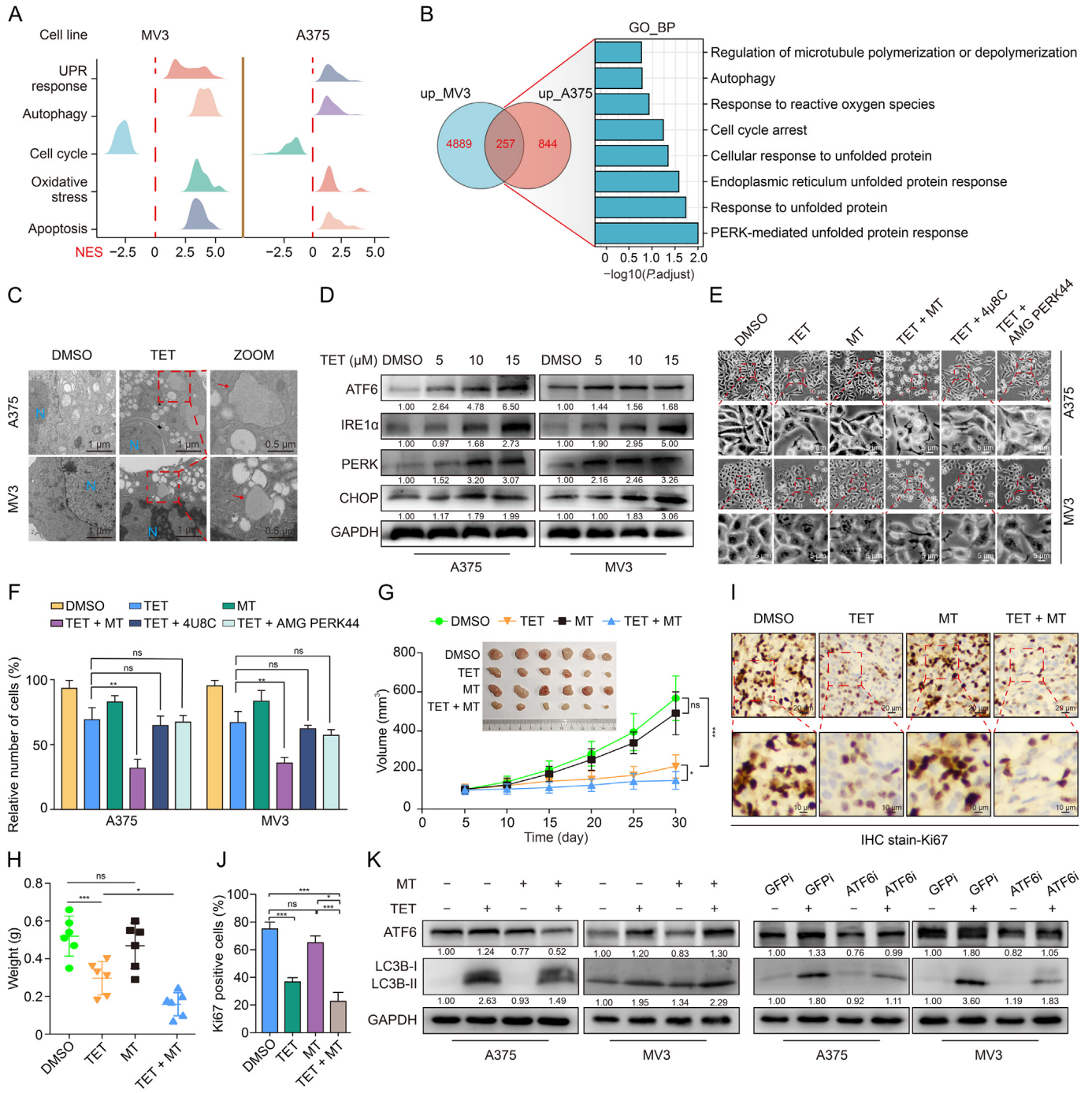

Fig. 3. Tetrandrine (TET) induced autophagy via triggering endoplasmic reticulum (ER) stress. (A) The mountainous plots showed the co-enriched pathways between MV3 and A375 cell lines in gene set enrichment analysis (GSEA). (B) Left: Venn plots presented the co-upregulated genes after treated with TET. Right: Gene ontology (GO) enrichment revealed the relevant biological processes enriched in these genes. (C) The morphology of endoplasmic reticulum (ER) in A375 and MV3 cells were observed under transmission electron microscopy (TEM) after treated with DMSO or TET (10 μM) for 48 h. (D) Western blot assay detected the expression of ER stress-related proteins in A375 and MV3 cells after treated with DMSO or TET (5, 10, and 15 μM) for 48 h. (E, F) Cell morphology of A375 and MV3 cells was observed after treated with TET and a series of ER-stress pathway inhibitors (melatonin (MT), 4μ8C, and AMG PERK 44) for 48 h (Drug concentrations: 2 μM MT, 4 μM 4μ8C, and 6 nM AMG PERK44 for A375 cells and 5 μM MT, 4 μM 4μ8C, and 6 nM AMG PERK44 for MV3 cells, respectively; 5 μM for TET added to both cells.) (E), and cell numbers of A375 and MV3 cells were respectively counted (F). (G, H) After subcutaneously injecting melanoma cell into mice, they were treated by intraperitoneally injecting DMSO, TET (120 mg/kg), MT (60 mg/kg), and TET + MT (120 mg/kg+60 mg/kg), qod, 30 days in total. The xenograft tumors ($n = 6$) were dissected, weighed and volume measured after 30 days treatment period. (I, J) The expression of Ki67 in xenograft tumor tissues among different treatment groups was detected by immunocytochemistry (IHC) assay and quantified. (K) Western blot assay detected the expression of activating transcription factor 6 (ATF6) and LC3B after treated with TET in ATF6 depletion and control cells. All data were analyzed by unpaired Student's *t*-tests and are shown as the means ± standard deviation (SD). $^{*}P < 0.05$, $^{**}P < 0.01$, $^{***}P < 0.001$, ns: not statistically significant. UPR: unfolded protein response; DMSO: dimethyl sulfoxide; IRE1α: inositol requiring enzyme 1 alpha; CHOP: CCAAT/enhancer-binding protein homologous protein; GAPDH: glyceraldehyde-3-phosphate dehydrogenase; PI: propidium iodide; GFPi: green fluorescent protein interfering; ATF6i: ATF6 interfering.

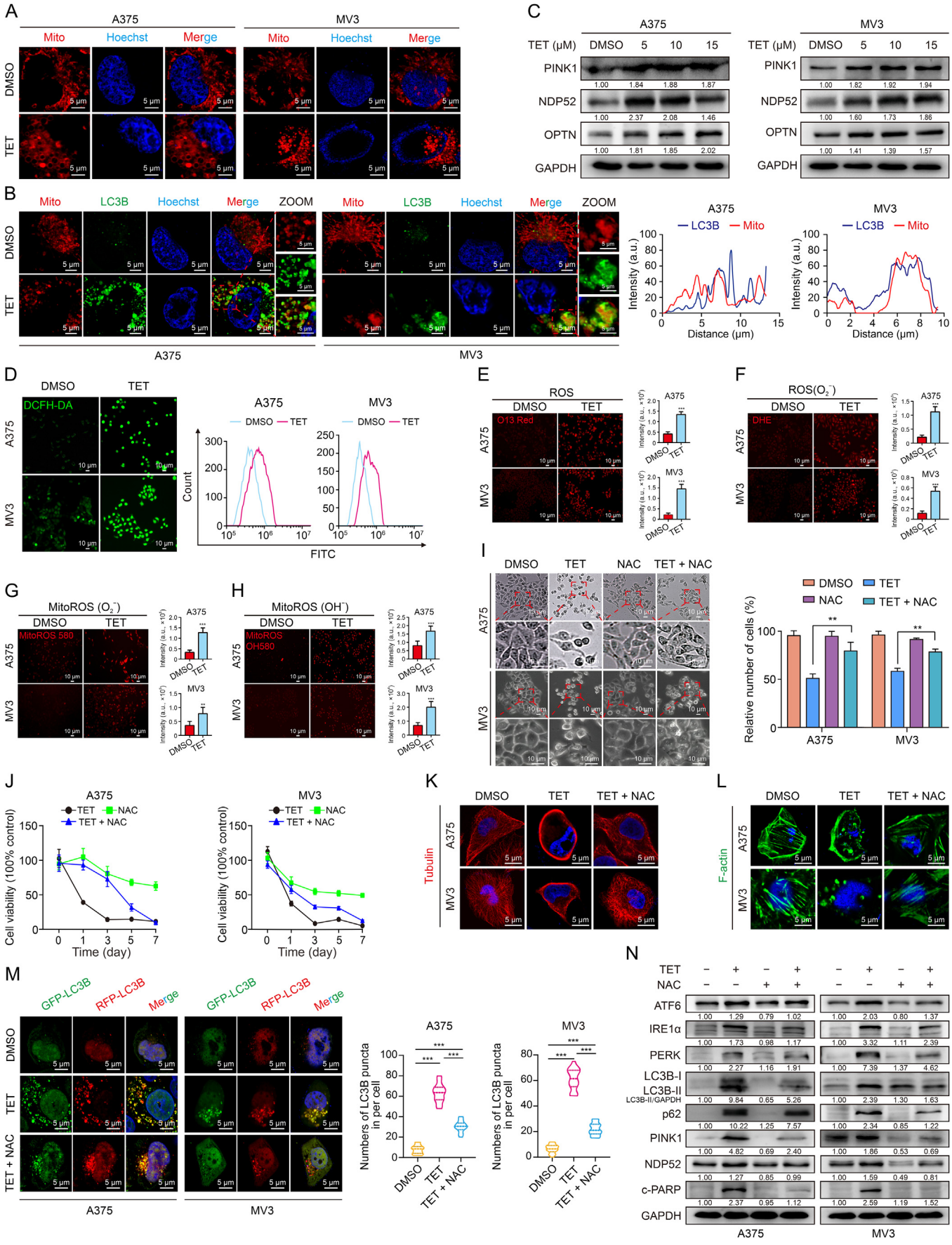
A
A375
MV3
Mito
Hoechst
Merge
DMSO
TET
5 μm
C
TET (μM)
DMSO
5
10
15
PINK1
NDP52
OPTN
GAPDH
1.00 1.84 1.88 1.87
1.00 2.37 2.08 1.46
1.00 1.81 1.85 2.02
1.00 1.82 1.92 1.94
1.00 1.60 1.73 1.86
1.00 1.41 1.39 1.57
B
LC3B
ZOOM
Intensity (a.u.)
Distance (μm)
D
DCFH-DA
Count
FITC
E
ROS
O13 Red
F
ROS(O2−)
DHE
G
MitoROS (O2−)
MitoROS 580
H
MitoROS (OH−)
MitoROS OH580
I
NAC
TET + NAC
Relative number of cells (%)
J
Cell viability (100% control)
Time (day)
K
Tubulin
L
F-actin
M
GFP-LC3B
RFP-LC3B
Merge
Numbers of LC3B puncta in per cell
N
ATF6
IRE1α
PERK
LC3B-I
LC3B-II
LC3B-II/GAPDH
p62
PINK1
NDP52
c-PARP
GAPDH

notable decrease in both tumor volume and weight (Figs. 6I and J). In addition, downregulation of the proliferative Ki67 marker within xenografts was observed, coupled with SIRT5 inhibition in the TET-treated groups, using an IHC assay (Fig. 6K). Intriguingly, TET failed to inhibit the proliferative and tumorigenic abilities when SIRT5 was overexpressed in melanoma cells (Figs. 6I–K), indicating that TET might target SIRT5 to exert its anti-cancer effect. These findings show that TET has an excellent antitumor effect in mouse models and underscore the pivotal role of SIRT5 as the likely target mediating the anti-melanoma effects exerted by TET.

4. Discussion

The potential of traditional Chinese medicine in tumor treatment has been gradually revealed, propelling in-depth investigations into the antitumor activity of monomers extracted from traditional Chinese herbs (MCTHs). Among these, *Stephania tetrandra* S. Moore stands out, with a legacy spanning over 2000 years, demonstrating both safety and efficacy. TET, a plant alkaloid derived from *S. tetrandra*, has emerged as a promising candidate for anti-cancer treatment.

While traditional studies have considered TET as a chemotherapeutic agent owing to its potential cellular toxicity and non-specific targets, its precise mechanism and molecular targets in anti-melanoma progression remain unclear. Our current study has unveiled a groundbreaking mechanism that bridges this gap by revealing the binding affinity of TET for SIRT5. SIRT5, a mitochondrial sirtuin deacylase, exhibits diverse enzymatic activities, including NAD^+-dependent demalonylation, desuccinylation, and deglutarylation [22]. SIRT5 plays a pivotal role in cellular metabolism, encompassing the tricarboxylic acid (TCA) cycle, electron transport chain, glycolysis, fatty acid oxidation, ketone body formation, nitrogenous waste management, and ROS detoxification [23]. Moreover, SIRT5 influences mitochondrial dynamics, affecting fission and fusion processes [24]. Our findings not only shed light on the interaction between TET and SIRT5 but also emphasize the multifaceted functions of SIRT5 in crucial cellular processes. Unraveling the intricate mechanisms underlying these interactions opens new avenues for understanding the potential therapeutic applications of traditional herbal compounds in targeted cancer treatment.

Significantly, our investigation revealed a heightened expression of SIRT5 in melanoma, correlating with a poorer prognosis. Likewise, a $Sirt5^{-/-}$ knockout murine melanoma model ($Tyr^{Cre\ ERT\ 2/+}$; $Braf^{LSL\text{-}V600E/+}$; $Pten^{flox/flox}$) showed that SIRT5 is dispensable for $Braf^{V600E}$-mediated melanoma formation and growth [25]. Another study showed that SIRT5 supports the viability of melanoma cells by affecting chromatin dynamics, including the maintenance of histone acetylation and methylation levels, thereby promoting proper gene expression [26]. These findings indicate that SIRT5 is an important drug target in melanoma treatment. Up to now, many efforts also have been made for the screening and developing SIRT5 inhibitors [22]. Our research identified that TET could bind to SIRT5 protein, inducing its concentration-dependent destabilization, potentially through the proteasomal system. This establishes TET as a prospective SIRT5 inhibitor, suggesting its potential as an anticancer drug specifically for SIRT5-overexpressed tumors.

Previous studies have shown that TET targets other proteins. For instance, in cervical cancer, TET has been shown to target the ether-à-go-go potassium channel 1 (Eag1) [27]. Notably, Eag1 expression has been observed in selected melanoma cell lines, suggesting a potential avenue for the action in these contexts [28]. Intriguingly, potassium channels such as BK and KCa3.1, when activated by intracellular calcium elevation, have been associated with augmenting the metastatic potential of melanoma cells [29]. Moreover, TET has been identified as a novel inhibitor of protein kinase c (PKC)-α in breast cancer cells [30]. This indicates that the effect of TET on melanoma may partially depend on other targets.

In this study, we demonstrated that TET induces a spectrum of cellular responses in melanoma, including apoptosis, G2M phase cell cycle arrest, autophagy, mitophagy, ER stress, ROS accumulation, and cytoskeletal protein depolymerization. Interestingly, similar phenotypes have been observed in other cancer cells treated with TET, underscoring the broad impact across various cancer types.

TET induces apoptosis in various cancer types including nasopharyngeal carcinoma, oral cancer, glioma, neuroblastoma, leukemia, liposarcoma, lung cancer, breast cancer, hepatocellular carcinoma, hepatoblastoma, pancreatic cancer, gastric cancer, colorectal cancer, gallbladder carcinoma, bladder cancer, renal cell carcinoma, cervical cancer, and endometrial cancer. In the current study, we observed the cleavage and activation of PARP and caspase3, corroborating TET-induced apoptosis.

The effects of TET on cell cycle arrest are pervasive in various cancers. While TET treatment led to G0/G1 phase arrest in numerous tumors, such as laryngeal cancer, breast cancer, leukemia, osteosarcoma, lung cancer, pancreatic cancer, colorectal cancer, ovarian cancer, renal cancer, and gallbladder carcinoma, G2M phase arrest was observed solely in hepatocellular carcinoma and melanoma in our study.

Autophagy also emerges as a significant player in TET-treated cancer cells [30], demonstrating activation across several cancer types, including nasopharyngeal carcinoma, oral cancer, triple-negative breast cancer, acute megakaryoblastic leukemia, primary leukemia of M5 type patients, pituitary adenoma, liver cancer, pancreatic cancer, gastric cancer, bladder cancer, and prostate cancer. The modulation of autophagy pathways by TET varies among these cancers. In most instances, autophagy activation involves signaling pathways such as beclin-1/LC3-I and II, which are

Fig. 4. Tetrandrine (TET) brought about mitophagy and massive reactive oxygen species (ROS) accumulation. (A) Mitochondria (Mito) morphology in both A375 and MV3 cells was observed after treated with dimethyl sulfoxide (DMSO) and TET (10 μM) for 48 h. (B) Left: The co-localizations between mitochondria (red) and LC3B (green) in A375 and MV3 cells were detected by using immunofluorescence (IF) assay after treated with DMSO or TET (10 μM) for 48 h. Right: The intensity of green and red signals in melanoma cells per slide was calculated by ImageJ software. (C) Western blot assay detected the expressions of mitophagy-related proteins after treated with TET (5, 10 and 15 μM) for 48 h and DMSO. (D) Intracellular ROS levels was evaluated by using dichlorodihydrofluorescein (DCFH)-diacetate (DA)-associated fluorescent imaging (left) and flow cytometry (right) after treated with TET (10 μM). (E–H) The levels of intracellular ROS (E), intracellular superoxide anion (F), mitochondrial superoxide anion (G), and mitochondrial hydroxyl radicals (H) in melanoma cells after treated with TET (10 μM) were respectively evaluated by O13 Red, dihydroethidium (DHE), MitoROS 580, and MitoROS OH580 probes. (I, J) Left: Cell morphology of A375 and MV3 cells was observed after respectively treated with DMSO, TET (10 μM), N-acetylcysteine (NAC) (20 μM), or TET + NAC for 48 h. Right: Cell numbers of MV3 and A375 cells were counted (I), and the viability of A375 and MV3 cells was also assessed by 3-(4,5-dimethylthiazol-2-yl)-2,5-diphenyl tetrazolium bromide (MTT) method (J). (K, L) The morphological structures of microtubule (tubulin antibody) (K) and microfilaments (phalloidin dyes) (L) was detected by IF assay in A375 and MV3 cells after treated with DMSO, TET (10 μM), NAC (20 μM) or TET + NAC for 48 h. (M) After transfected with green fluorescent protein (GFP)-red fluorescent protein (RFP)-LC3 plasmids, the level of autophagy was detected by IF assay in A375 and MV3 cells after treated with DMSO, TET (10 μM), NAC (20 μM) or TET + NAC for 48 h. (N) Western blot detected the expressions of ER stress, autophagy, and apoptosis markers in A375 and MV3 cells after treated with DMSO, TET (10 μM), NAC (20 μM) or TET + NAC for 48 h. All data were analyzed by unpaired Student's *t*-tests and are shown as the means ± standard deviation (SD). $^{**}P < 0.01$, $^{***}P < 0.001$. PERK: double-stranded RNA-dependent protein kinase-like ER kinase; IRE1α: inositol requiring enzyme 1 alpha; PINK1: phosphatase and tensin homolog (PTEN)-induced kinase 1; NDP52: nuclear dot protein 52 kDa; OPTN: optineurin; c-PARP: cleaved poly (ADP-ribose) polymerase; ATF6: activating transcription factor 6; GAPDH: glyceraldehyde-3-phosphate dehydrogenase.

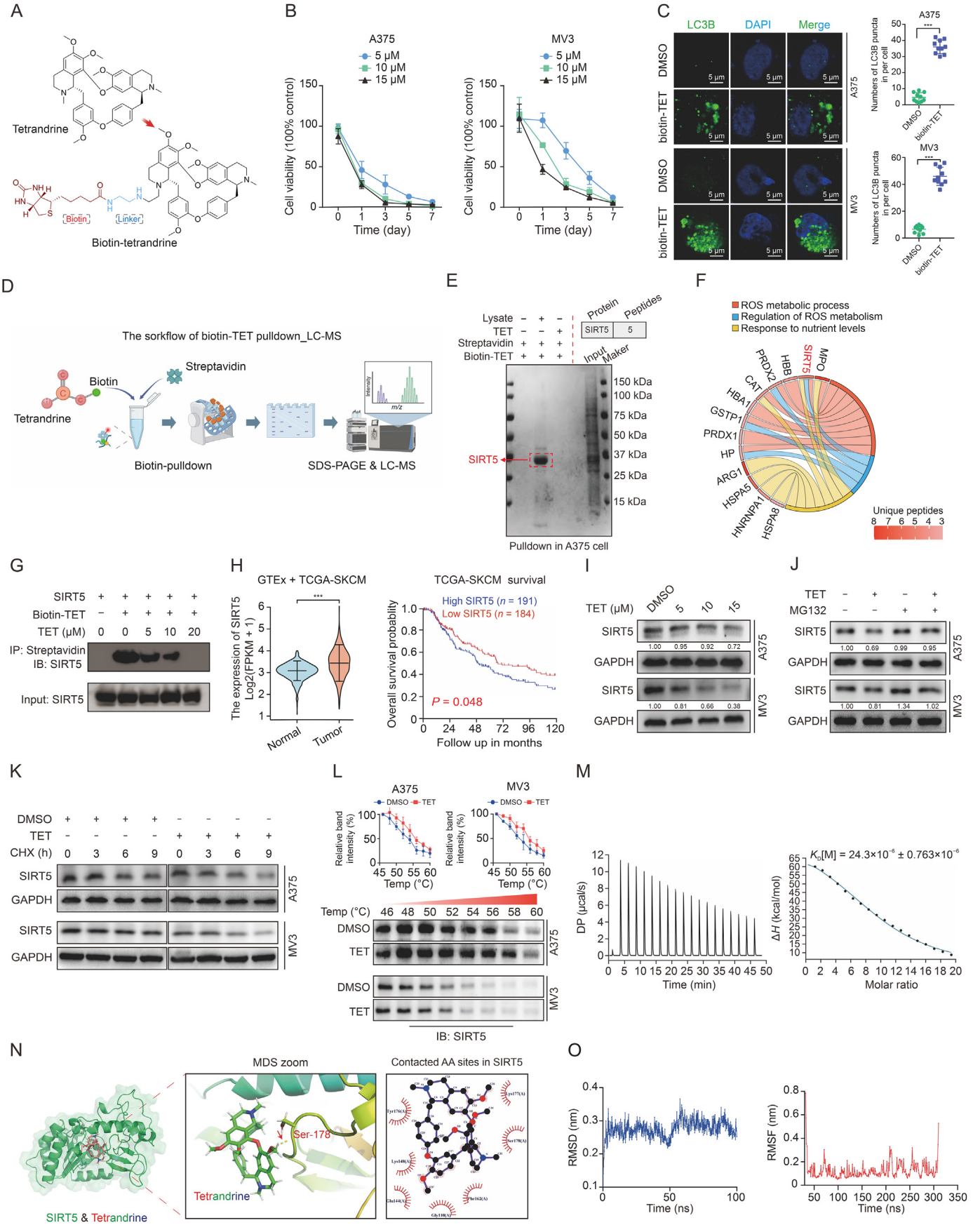
A
Tetrandrine
Biotin
Linker
Biotin-tetrandrine
B
A375
MV3
5 μM
10 μM
15 μM
Cell viability (100% control)
Time (day)
C
LC3B
DAPI
Merge
DMSO
biotin-TET
A375
MV3
Numbers of LC3B puncta in per cell
D
The sorkflow of biotin-TET pulldown_LC-MS
Biotin
Streptavidin
Tetrandrine
Biotin-pulldown
SDS-PAGE & LC-MS
E
Lysate
TET
Streptavidin
Biotin-TET
Protein
Peptides
SIRT5
Input
Maker
150 kDa
100 kDa
75 kDa
50 kDa
37 kDa
25 kDa
15 kDa
Pulldown in A375 cell
F
ROS metabolic process
Regulation of ROS metabolism
Response to nutrient levels
SIRT5
MPO
HBB
PRDX2
CAT
HBA1
GSTP1
PRDX1
HP
ARG1
HSPA5
HNRNPA1
HSPA8
Unique peptides
G
SIRT5
Biotin-TET
TET (μM)
IP: Streptavidin
IB: SIRT5
Input: SIRT5
H
GTEx + TCGA-SKCM
The expression of SIRT5 Log2(FPKM + 1)
Normal
Tumor
TCGA-SKCM survival
High SIRT5 (n = 191)
Low SIRT5 (n = 184)
P = 0.048
Overall survival probability
Follow up in months
I
TET (μM)
DMSO
SIRT5
GAPDH
A375
MV3
J
TET
MG132
K
DMSO
TET
CHX (h)
L
A375
MV3
Relative band intensity (%)
Temp (°C)
IB: SIRT5
M
DP (μcal/s)
Time (min)
K_D[M] = 24.3×10⁻⁶ ± 0.763×10⁻⁶
ΔH (kcal/mol)
Molar ratio
N
MDS zoom
Contacted AA sites in SIRT5
Ser-178
Tetrandrine
SIRT5 & Tetrandrine
O
RMSD (nm)
Time (ns)
RMSF (nm)

mediated through diverse mechanisms. These mechanisms include PKC-α inhibition, PI3K/AKT/mTOR-dependent pathways in a calcium/calmodulin-dependent protein kinase kinase-β (CaMKK-β)/5' AMPK-independent manner [31], or through AMPK-dependent pathways [14]. Interestingly, TET exerts diverse effects on autophagy in different cell lines. In DU145 cells, TET neutralizes lysosomal acidity and blocks autophagy, independent of LC3 conversion [32]. In contrast, in other studies, TET induced lysosomal deacidification, thereby hindering autophagic flux in the degradation stage; this process relied on LC3 conversion [33]. Furthermore, TET inactivated lysosomes [34]. In the current study, we observed that TET blocked autophagic flux, as evidenced by increased p62 levels. Importantly, mitophagy has been reported in both cancerous and non-tumorigenic cells [35]. Notably, TET-induced ER stress has also been observed in other cancer cells, such as nasopharyngeal carcinoma and liposarcoma. The effect of TET on cytoskeletal protein depolymerization has also been observed in various studies. Previous studies have reported microtubule aggregation in brain cell homogenates from guinea pigs [36]. In human gastric cancer cell lines, TET significantly reduced mRNA expression of β-tubulin III [37]. Additionally, TET decreased the expression of α-smooth muscle actin (α-SMA) via the TGF-β1 signaling pathway, preventing pulmonary fibrosis [38]. Moreover, TET reduced α-SMA expression in the HSC-T6 rat hepatic stellate cell line following tumor necrosis factor-α (TNF-α) treatment at a lower concentration (6.25 μM) [39]. Suppressive effect of TET on actin ring formation prevents bone loss in ovariectomized mice [40]. This study is the first to identify depolymerization of cytoskeletal proteins, including tubulin and F-actin, in cancer cells following TET treatment, representing a novel observation in this context.

The relationship between phenotypes induced by TET in cancer cells reveals a complex interplay. Studies have demonstrated the contrasting roles of autophagy in TET-induced apoptosis in different cancer types. For instance, autophagy enhances TET-induced apoptosis in bladder cancer cells and pituitary adenomas [14]. Conversely, in gastric cancer, autophagy inhibition alleviates TET-induced apoptosis. This variability suggests the existence of context-specific interactions between autophagy and TET-mediated apoptosis. Autophagy is closely linked to cytoskeleton. Depolymerization of the cytoskeleton, possibly induced by TET, may contribute to autophagy.

Furthermore, TET treatment triggers ROS accumulation in diverse cancer types, including nasopharyngeal carcinoma, oral cancer, glioma, breast cancer, leukemia, hepatocellular carcinoma, pancreatic cancer, and prostate cancer. TET-induced autophagy is believed to be initiated via activation of the Notch 1 and AKT signaling pathways, leading to ROS accumulation [41]. In turn, ROS activates the extracellular signal-regulated kinase (ERK) signaling pathway, partially contributing to TET-induced autophagy [42]. Additionally, ROS accumulation has been implicated in caspase-dependent apoptosis in breast and pancreatic cancer cells [43], and in G0/G1 cell cycle arrest in mouse endothelial cells following TET treatment [44]. In the current study, ROS accumulation induced by TET served as a central mechanism triggering ER stress, autophagy, mitophagy, and cytoskeletal protein depolymerization. The build-up of ROS due to TET exposure likely leads to an abundance of oxidized molecules, including proteins. These oxidized molecules contribute to ER stress, subsequently initiating ER-phagy, and inducing autophagy and mitophagy. Previous studies indicated that ROS production is predominantly triggered by damaged mitochondria [45]. Our investigation revealed that TET treatment induced mitochondrial damage, resulting in mitochondrial swelling and subsequent mitophagy. Additionally, previous research has highlighted that TET-mediated blockade of autophagic flux leads to insufficient substrates for the TCA cycle and impaired oxidative phosphorylation (OxPhos) [33]. This suppression of mitochondrial ATP production intensifies cytotoxicity in human lung carcinoma A549 cells upon TET exposure [46].

Importantly, we identified SIRT5, a member of the sirtuin family that is localized within the mitochondria, as the primary target of TET. Notably, SIRT5 plays a pivotal role in mitochondrial metabolism and modulates mitochondrial fusion/fission dynamics [47]. Furthermore, the enzymatic actions of SIRT5 extend to the desuccinylation and activation of SOD1, enabling ROS scavenging [48]. Additionally, SIRT5 can desuccinylate IDH2 and deglutarylate G6PD, thereby enhancing the cellular antioxidant defense mechanisms [49]. Interestingly, SIRT5 induces ammonia production via glutaminase desuccinylation, which is associated with cellular autophagy and mitophagy [50].

In conclusion, our study demonstrated that TET effectively targets SIRT5, precipitating SIRT5 protein degradation. This cascade of events leads to mitochondrial dysfunction, which manifests as mitochondrial swelling, mitophagy, and subsequent ROS generation. The ensuing cellular responses included ER stress, cytoskeletal depolymerization, autophagy, apoptosis, and G2M phase cell cycle arrest. This comprehensive elucidation provides a systematic understanding of the primary mechanisms driving the diverse phenotypes induced by TET in melanoma. The compelling evidence presented here indicates that TET is a promising therapeutic agent for the treatment of melanoma. These findings pave the way for the further exploration and development of TET-based strategies to address the complexities of melanoma progression.

Fig. 5. Sirtuin 5 (SIRT5) was identified as a direct target of tetrandrine (TET). (A) Chemical structure of TET and synthetic biotin-TET. (B) Cell viability of A375 and MV3 cells after treated with different concentrations of biotin-TET was measured by 3-(4,5-dimethylthiazol-2-yl)-2,5-diphenyl tetrazolium bromide (MTT) method. (C) The expression of LC3B was detected after treated with biotin-TET by immunofluorescence (IF) assay. (D, E) SIRT5 was screened out through biotin-TET pulldown and liquid chromatography-mass spectrometry (LC-MS). (F) Gene Expression Omnibus (GEO) enrichment analysis showed that the proteins interacted with biotin-TET mainly were enriched in the 3 following pathways: reactive oxygen species (ROS) metabolic process, regulation of ROS metabolic process, and response to nutrient levels. (G) Chemical competitive binding experiment: after the incubation of biotin-TET and recombinant SIRT5 protein, TET with different concentrations was respectively added into the tube and strep-pulldown SIRT5 was detected by Western blot assay. (H) The bioinformatic analysis of SIRT5 in The Cancer Genome Atlas (TCGA) and Genotype-Tissue Expression (GTEx) databases. (I) Western blot assay detected the expression of SIRT5 in MV3 and A375 cells after treated with different TET concentrations (5, 10 and 15 μM) for 48 h. (J) After cells were treated with TET or dimethyl sulfoxide (DMSO), MG132 was added for 8 h to probe into whether the degradation of SIRT5 via the ubiquitin (Ub)-26S proteasome system (UPS). (K) After cells treated with 10 μM TET or DMSO, cycloheximide (CHX, 100 μg/mL) was added at indicated time points for the purpose of detecting half-time of SIRT5. (L) Cellular thermal shift assay demonstrated that TET could bind to SIRT5 in melanoma cells. (M) Isothermal titration calorimetry (ITC) analysis demonstrated that TET could directly bind to recombinant SIRT5 protein. (N) Molecular dynamics simulation (MDS) revealed the specific interacted pattern between TET and SIRT5. (O) Atomic root mean square deviation (RMSD) measures the stability of the simulated system. Root mean square fluctuation (RMSF) reflects the local site deformation of the system during the simulation process. All data were analyzed by unpaired Student's *t*-tests and are shown as the means ± standard deviation (SD). $^{***}P < 0.001$. Temp: temperature; SDS-PAGE: sodium dodecyl sulfate-polyacrylamide gel electrophoresis; GAPDH: glyceraldehyde-3-phosphate dehydrogenase.

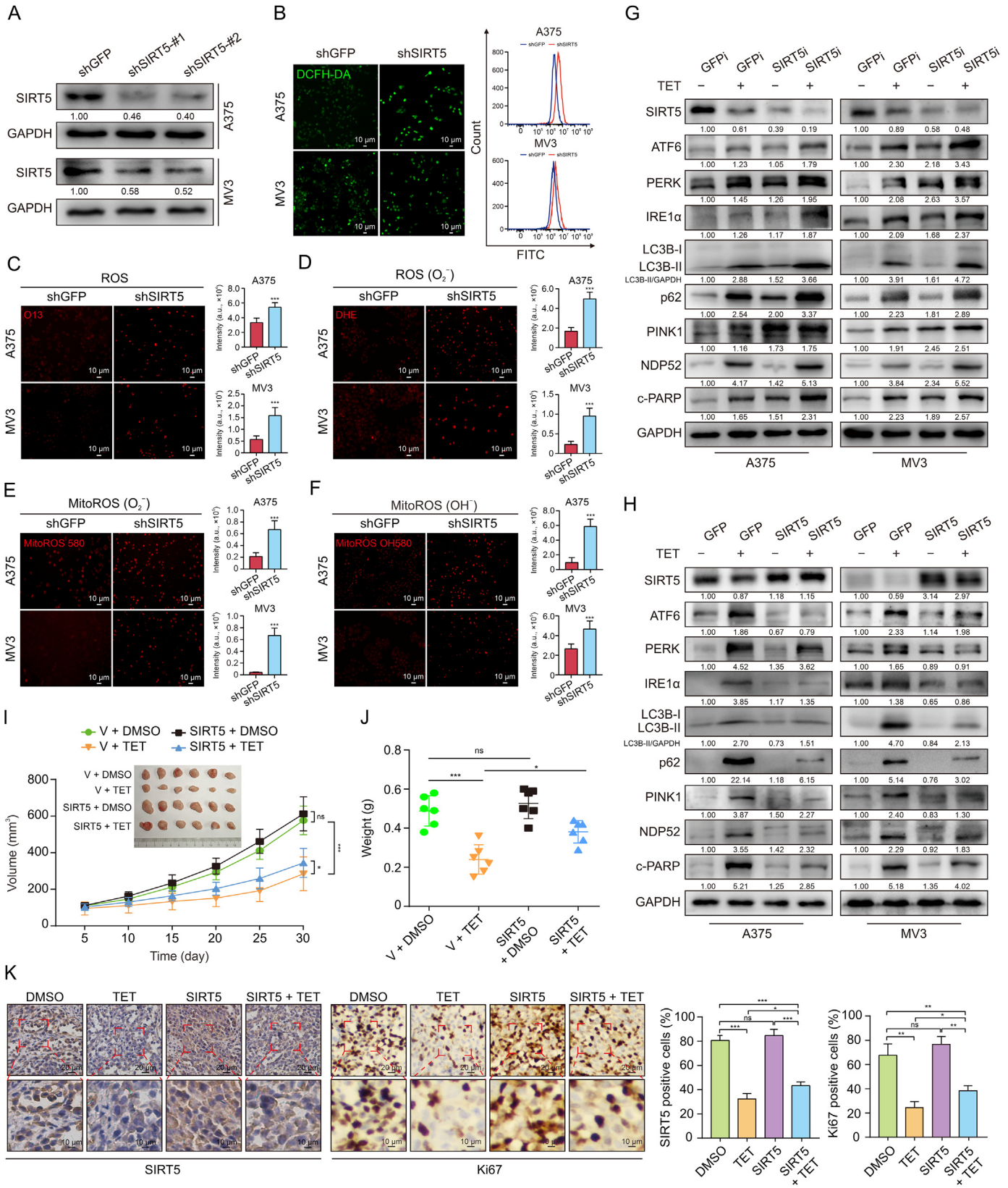

Fig. 6. Sirtuin 5 (SIRT5) depletion cooperating with tetrandrine (TET) treatment accelerated melanoma cell death. (A) The knockdown efficiency of two SIRT5 shRNA fragments was evaluated in A375 and MV3 cells by Western blot assay. (B) Reactive oxygen species (ROS) level was detected by utilizing immunofluorescence (IF) and flow cytometry. (C–F) The levels of intracellular ROS (C), intracellular superoxide anion (D), mitochondrial superoxide anion (E), and mitochondrial hydroxyl radicals (F) in shGFP and SIRT5 depletion melanoma cells were respectively evaluated by O13 Red, dihydroethidium (DHE), MitoROS 580, and MitoROS OH580 probes. (G, H) Western blot assay detected the expressions of endoplasmic reticulum (ER) stress, autophagy, mitophagy and apoptosis associated proteins between shGFP vs. shSIRT5 and OE-GFP vs. OE-SIRT5 groups after treated with dimethyl

CRediT authorship contribution statement

Yacong Ji: Conceptualization, Data curation, Methodology, Software, Supervision, Validation, Writing – original draft, Formal analysis, Visualization, Writing – review & editing. **Chongyang Li:** Conceptualization, Methodology, Supervision, Validation, Visualization, Data curation, Formal analysis, Writing – review & editing. **Sicheng Wan:** Methodology, Software, Formal analysis, Visualization, Writing – review & editing. **Zhen Dong:** Methodology, Visualization, Writing – review & editing. **Chaolong Liu:** Data curation, Validation. **Leiyang Guo:** Data curation, Validation. **Shaomin Shi:** Data curation, Validation. **Mingxin Ci:** Data curation, Validation. **Minghao Xu:** Data curation, Validation. **Qian Li:** Data curation, Validation. **Huanrong Hu:** Data curation, Validation. **Hongjuan Cui:** Conceptualization, Funding acquisition, Writing – review & editing, Resources. **Yaling Liu:** Conceptualization, Funding acquisition, Resources, Supervision.

Declaration of competing interest

The authors declare that there are no conflicts of interest.

Acknowledgments

This work was supported by funding from Natural Science Foundation of China (Grant Nos.: 82372519 and 81902664), the Postdoctoral Fellowship Program of CPSF (Grant No.: GZB20240544), the China Postdoctoral Science Foundation (Grant No.: 2024M752432), the Natural Science Foundation of Hebei Province (Grant Nos.: H2022206368 and H2022206446), Medical Science Research Program of the Hebei Provincial Health Commission (Grant No.: 20241603), and Pilot Program of Southwest University (Program No.: SWU-XDZD22006). We also thanked Jifu Li from the College of Sericulture and Textile and Biomass Science of Southwest University for the assistance during the use of the confocal fluorescence microscope (FV1000, Olympus, Japan).

Appendix A. Supplementary data

Supplementary data to this article can be found online at https://doi.org/10.1016/j.jpha.2024.101036.

References

[1] R.L. Siegel, K.D. Miller, H.E. Fuchs, et al., Cancer statistics, 2022, CA A Cancer, J. Clin. 72 (2022) 7–33.
[2] M. Chanda, M.S. Cohen, Advances in the discovery and development of melanoma drug therapies, Expert Opin. Drug Discov. 16 (2021) 1319–1347.
[3] B.E. Nelson, J. Roszik, F. Janku, et al., BRAF v600E-mutant cancers treated with vemurafenib alone or in combination with everolimus, sorafenib, or crizotinib or with paclitaxel and carboplatin (VEM-PLUS) study, NPJ Precis. Oncol. 7 (2023), 19.
[4] J. Guo, R.D. Carvajal, R. Dummer, et al., Efficacy and safety of nilotinib in patients with KIT-mutated metastatic or inoperable melanoma: Final results from the global, single-arm, phase II TEAM trial, Ann. Oncol. 28 (2017) 1380–1387.
[5] J.Y. Blay, L. Shen, Y.K. Kang, et al., Nilotinib versus imatinib as first-line therapy for patients with unresectable or metastatic gastrointestinal stromal tumours (ENESTg1): A randomised phase 3 trial, Lancet Oncol. 16 (2015) 550–560.
[6] R. Roskoski Jr., Allosteric MEK1/2 inhibitors including cobimetanib and trametinib in the treatment of cutaneous melanomas, Pharmacol. Res. 117 (2017) 20–31.
[7] A. Boespflug, L. Thomas, Cobimetinib and vemurafenib for the treatment of melanoma, Expert Opin. Pharmacother. 17 (2016) 1005–1011.
[8] F. Abdi, E. Arkan, M. Eidizadeh, et al., The possibility of angiogenesis inhibition in cutaneous melanoma by bevacizumab-loaded lipid-chitosan nanoparticles, Drug Deliv. Transl. Res. 13 (2023) 568–579.
[9] J.R. Brahmer, C. Lacchetti, B.J. Schneider, et al., National Comprehensive Cancer Network, Management of immune-related adverse events in patients treated with immune checkpoint inhibitor therapy: American society of clinical oncology clinical practice guideline, J. Clin. Oncol. 36 (2018) 1714–1768.
[10] C. Fellner, Ipilimumab (yervoy) prolongs survival in advanced melanoma: Serious side effects and a hefty price tag may limit its use, P&T 37 (2012) 503–530.
[11] A. Zaremba, A.M.M. Eggermont, C. Robert, et al., The concepts of rechallenge and retreatment with immune checkpoint blockade in melanoma patients, Eur. J. Cancer 155 (2021) 268–280.
[12] H. Zou, T. He, X. Chen, Tetrandrine inhibits differentiation of proinflammatory subsets of T helper cells but spares *de novo* differentiation of iTreg cells, Int. Immunopharmacol. 69 (2019) 307–312.
[13] W.-X. Yao, M.-X. Jiang, Effects of tetrandrine on cardiovascular electrophysiologic properties, Acta Pharmacol. Sin. 23 (2002) 1069–1074.
[14] B. Kou, W. Liu, X. Xu, et al., Autophagy induction enhances tetrandrine-induced apoptosis via the AMPK/mTOR pathway in human bladder cancer cells, Oncol. Rep. 38 (2017) 3137–3143.
[15] G.N. van Muijen, K.F. Jansen, I.M. Cornelissen, et al., Establishment and characterization of a human melanoma cell line (MV3) which is highly metastatic in nude mice, Int. J. Cancer 48 (1991) 85–91.
[16] J. Du, Z. Dong, L. Tan, et al., Tubeimoside I inhibits cell proliferation and induces a partly disrupted and cytoprotective autophagy through rapidly hyperactivation of MEK1/2-ERK1/2 cascade via promoting PTP1B in melanoma, Front. Cell Dev. Biol. 8 (2020), 607757.
[17] G. Zhang, Q. Zhu, G. Fu, et al., TRIP13 promotes the cell proliferation, migration and invasion of glioblastoma through the FBXW7/c-MYC axis, Br. J. Cancer 121 (2019) 1069–1078.
[18] Y. Zhang, J. Hou, S. Shi, et al., CSN6 promotes melanoma proliferation and metastasis by controlling the UBR5-mediated ubiquitination and degradation of CDK9, Cell Death Dis. 12 (2021), 118.
[19] P. Holland, A. Simonsen, Actin shapes the autophagosome, Nat. Cell Biol. 17 (2015) 1094–1096.
[20] N. Mi, Y. Chen, S. Wang, et al., CapZ regulates autophagosomal membrane shaping by promoting actin assembly inside the isolation membrane, Nat. Cell Biol. 17 (2015) 1112–1123.
[21] D. Trisciuoglio, F. Degrassi, The tubulin code and tubulin-modifying enzymes in autophagy and cancer, Cancers (Basel) 14 (2021), 6.
[22] Y. Wang, H. Chen, X. Zha, Overview of SIRT5 as a potential therapeutic target: Structure, function and inhibitors, Eur. J. Med. Chem. 236 (2022), 114363.
[23] S. Kumar, D.B. Lombard, Functions of the sirtuin deacylase SIRT5 in normal physiology and pathobiology, Crit. Rev. Biochem. Mol. Biol. 53 (2018) 311–334.
[24] H. Guedouari, T. Daigle, L. Scorrano, et al., Sirtuin 5 protects mitochondria from fragmentation and degradation during starvation, Biochim. Biophys. Acta Mol. Cell Res. 1864 (2017) 169–176.
[25] H. Moon, J. Zhu, A.C. White, Sirt5 is dispensable for $Braf^{V600E}$-mediated cutaneous melanoma development and growth *in vivo*, Exp. Dermatol. 28 (2019) 83–85.
[26] W. Giblin, L. Bringman-Rodenbarger, A.H. Guo, et al., The deacylase SIRT5 supports melanoma viability by influencing chromatin dynamics, J. Clin. Invest. 131 (2021), e138926.
[27] X. Wang, Y. Chen, J. Li, et al., Tetrandrine, a novel inhibitor of ether-à-go-go-1 (Eag1), targeted to cervical cancer development, J. Cell. Physiol. 234 (2019) 7161–7173.
[28] R. Meyer, R. Schönherr, O. Gavrilova-Ruch, et al., Identification of ether à go-go and calcium-activated potassium channels in human melanoma cells, J. Membr. Biol. 171 (1999) 107–115.
[29] L. Ferrera, R. Barbieri, C. Picco, et al., TRPM2 oxidation activates two distinct potassium channels in melanoma cells through intracellular calcium increase, Int. J. Mol. Sci. 22 (2021), 8359.
[30] V.K.W. Wong, W. Zeng, J. Chen, et al., Tetrandrine, an activator of autophagy, induces autophagic cell death via PKC-α inhibition and mTOR-dependent mechanisms, Front. Pharmacol. 8 (2017), 351.
[31] Y. Guo, X. Pei, Tetrandrine-induced autophagy in MDA-MB-231 triple-negative breast cancer cell through the inhibition of PI3K/AKT/mTOR signaling, Evid. Based Complement. Alternat. Med. 2019 (2019), 7517431.
[32] W. Qiu, A.-L. Zhang, Y. Tian, Tetrandrine triggers an alternative autophagy in DU145 cells, Oncol. Lett. 13 (2017) 3734–3738.

sulfoxide (DMSO) or tetrandrine (TET) (10 μM) for 48 h. (I, J) After subcutaneously injecting the cells with stably overexpressing SIRT5 or green fluorescent protein (GFP) into mice, they were treated by TET (120 mg/kg/day), qod, 30 days in total. Tumor growth was daily monitored and measured every 5 days. The xenograft tumors ($n = 6$) were dissected, weighed and measured on the 30th day. (K) The expression of SIRT5 and Ki67 in xenograft tumor tissues was detected by immunocytochemistry (IHC) stain. The value of IHC positive signal in panels were quantified. All data were analyzed by unpaired Student's *t*-tests and are shown as the means ± standard deviation (SD). $^{*}P < 0.05$, $^{**}P < 0.01$, $^{***}P < 0.001$, ns: not statistically significant. DCFH-DA: dichlorodihydrofluorescein diacetate; GAPDH: glyceraldehyde-3-phosphate dehydrogenase; GFPi: GFP interfering; SIRT5i: SIRT5 interfering; ATF6: activating transcription factor 6; PERK: double-stranded RNA-dependent protein kinase-like ER kinase; IRE1α: inositol requiring enzyme 1 alpha; PINK1: phosphatase and tensin homolog (PTEN)-induced kinase 1; NDP52: nuclear dot protein 52 kDa; c-PARP: cleaved poly (ADP-ribose) polymerase; V: vector.

[33] W. Qiu, M. Su, F. Xie, et al., Tetrandrine blocks autophagic flux and induces apoptosis via energetic impairment in cancer cells, Cell Death Dis. 5 (2014), e1123.
[34] E. Sato, S. Ohta, K. Kawakami, et al., Tetrandrine increases the sensitivity of human lung adenocarcinoma PC14 cells to gefitinib by lysosomal inhibition, Anticancer Res 39 (2019) 6585–6593.
[35] H. Wang, T. Liu, L. Li, et al., Tetrandrine is a potent cell autophagy agonist via activated intracellular reactive oxygen species, Cell Biosci. 5 (2015), 4.
[36] L.F. Liu, N.M. Chen, G.P. Cai, et al., Studies on the effect of tetrandrine on microtubules. I. Biochemical observation and electron microscopy, Ecotoxicol. Environ. Saf. 15 (1988) 142–148.
[37] J. Wei, B. Liu, L. Wang, et al., Synergistic interaction between tetrandrine and chemotherapeutic agents and influence of tetrandrine on chemotherapeutic agent-associated genes in human gastric cancer cell lines, Cancer Chemother. Pharmacol. 60 (2007) 703–711.
[38] Y. Liu, W. Zhong, J. Zhang, et al., Tetrandrine modulates rheb-mTOR signaling-mediated selective autophagy and protects pulmonary fibrosis, Front. Pharmacol. 12 (2021), 739220.
[39] X. Li, Q. Jin, Y.-L. Wu, et al., Tetrandrine regulates hepatic stellate cell activation via TAK1 and NF-κB signaling, Int. Immunopharmacol. 36 (2016) 263–270.
[40] Z. Zhong, Z. Qian, X. Zhang, et al., Tetrandrine prevents bone loss in ovariectomized mice by inhibiting RANKL-induced osteoclastogenesis, Front. Pharmacol. 10 (2019), 1530.
[41] G. Wu, T. Liu, H. Li, et al., C-MYC and reactive oxygen species play roles in tetrandrine-induced leukemia differentiation, Cell Death Dis. 9 (2018), 473.
[42] K. Gong, C. Chen, Y. Zhan, et al., Autophagy-related gene 7 (ATG7) and reactive oxygen species/extracellular signal-regulated kinase regulate tetrandrine-induced autophagy in human hepatocellular carcinoma, J. Biol. Chem. 287 (2012) 35576–35588.
[43] N. Bhagya, K.R. Chandrashekar, A. Prabhu, et al., Tetrandrine isolated from Cyclea peltata induces cytotoxicity and apoptosis through ROS and caspase pathways in breast and pancreatic cancer cells, In Vitro Cell. Dev. Biol. Anim. 55 (2019) 331–340.
[44] W. Xiao, Y. Jiang, Q. Men, et al., Tetrandrine induces G1/S cell cycle arrest through the ROS/Akt pathway in EOMA cells and inhibits angiogenesis *in vivo*, Int. J. Oncol. 46 (2015) 360–368.
[45] Y. Yang, S. Karakhanova, W. Hartwig, et al., Mitochondria and mitochondrial ROS in cancer: Novel targets for anticancer therapy, J. Cell. Physiol. 231 (2016) 2570–2581.
[46] L.W.C. Chow, K.-S. Cheng, F. Leong, et al., Enhancing tetrandrine cytotoxicity in human lung carcinoma A549 cells by suppressing mitochondrial ATP production, Naunyn Schmiedebergs Arch, Pharmacol. 392 (2019) 427–436.
[47] S. Zhu, Z. Dong, X. Ke, et al., The roles of sirtuins family in cell metabolism during tumor development, Semin. Cancer Biol. 57 (2019) 59–71.
[48] Z.-F. Lin, H.-B. Xu, J.-Y. Wang, et al., SIRT5 desuccinylates and activates SOD1 to eliminate ROS, Biochem. Biophys. Res. Commun. 441 (2013) 191–195.
[49] L. Zhou, F. Wang, R. Sun, et al., SIRT5 promotes IDH2 desuccinylation and G6PD deglutarylation to enhance cellular antioxidant defense, EMBO Rep. 17 (2016) 811–822.
[50] L. Polletta, E. Vernucci, I. Carnevale, et al., SIRT5 regulation of ammonia-induced autophagy and mitophagy, Autophagy 11 (2015) 253–270.